Advanced Sensor Research

ADVANCED SENSOR RESEARCH Open Access

www.advsensorres.com

RESEARCH ARTICLE OPEN ACCESS

CNC-Printed Metasurface-Based Device for Potential Application in pH Sensing

Z. Viskadourakis[1] | M. Orfanou[2] | A. Pitilakis[3,4] | O. Tsilipakos[4] | E. Koudoumas[1,2,5] | G. Kenanakis[1]

[1]Institute of Electronic Structure and Laser (IESL), Foundation for Research and Technology – Hellas (FORTH), Heraklion, Greece | [2]Department of Electrical and Computer Engineering, Hellenic Mediterranean University, Heraklion, Greece | [3]School of Electrical and Computer Engineering, Aristotle University of Thessaloniki, Thessaloniki, Greece | [4]Theoretical and Physical Chemistry Institute, National Hellenic Research Foundation, Athens, Greece | [5]National Institute for R&D in Microtechnologies – IMT Bucharest, Bucharest, Romania

Correspondence: Z. Viskadourakis (zach@iesl.forth.gr)

Received: 31 March 2026 | **Revised:** 12 June 2026 | **Accepted:** 19 June 2026

Keywords: aqueous solution | cnc milling | dielectric permittivity | engraving | microwave sensor | network analyser | resonant sensor

ABSTRACT

In the current study, a microwave device based on a metasurface is investigated regarding its potential application as a pH sensor. The device was developed on a typical double-sided, Cu–coated FR-4 slide, utilizing the mechanical engraving method. It was electromagnetically characterized in the microwave band, i.e., 1–5 GHz. Furthermore, theoretical simulations were performed to confirm the measured electromagnetic response. Moreover, the fabricated device was tested against standard buffer solutions, such as those used for the calibration of conventional potentiometric pH meters, as well as against home-made acidic and basic aqueous solutions, with pH levels ranging from 2 up to 12. By analyzing the corresponding electromagnetic response, it is evident that the aforementioned pH device demonstrates a gradual response in varying pH levels. Furthermore, it exhibits adequate quality factor, sensitivity, and figure of merit values, indicating a measurable and application-relevant electromagnetic performance. Considering the above, it is evidently shown that the proposed metasurface–based device could be potentially used for the detection of pH levels in aqueous solutions.

1 | Introduction

As is known, pH is a logarithmic scale ranging from 0 to 14, through which the acidity/alkalinity of an aqueous solution can be quantified. It is directly related to the H^+ / OH^- ion concentration in the solution. For pH = 7, equal concentrations of H^+ and OH^- exist in the solution (neutral solution). For pH > 7, OH^- ions dominate (alkaline solution), while for pH < 7, H^+ cations are the majority ions (acidic solution).

The accurate pH measurement is essential in a great variety of applications. For example, monitoring and controlling the water pH levels gives important information about the water quality and its possible contamination [1–3]. Moreover, the measurement of the soil pH has an important impact in agriculture since it provides crucial information regarding the ability of the soil to absorb nutrients, while it also indicates any toxic metal contamination [1–5]. On the other hand, human blood pH level is strictly between 7.35 and 7.5, thus precise monitoring of the blood pH level improves human health, preventing diseases [6, 7]. In food science, pH directly affects the taste, texture, and conservation of foods. Hence, monitoring and control of pH in food products is essential since it is an indicator of the quality as well as safety levels that should be achieved during production and distribution of foods [8–10]. Lastly, in chemistry, precise knowledge and control of pH levels impacts chemical reactions [11, 12].

To date, potentiometric pH meters are the most common devices used to measure the acidity/alkalinity of aqueous solutions. In principle, a pH meter consists of a pH-sensitive electrode and a reference electrode [13]. When the device is immersed in a solution, a voltage drop develops between the electrodes, which is directly dependent on the ion concentration. By measuring this voltage drop, the device converts it in pH scale through a proper calibration. This method is easy to use; pH meters are compact and portable, thus they can be used for measurements outside the laboratory. However, they require regular calibration, using special buffer solutions, since an uncalibrated pH meter would give wrong measurements, far away from the real values. Moreover, the pH electrodes may exhibit degradation issues, losing their sensitivity through time. In addition, when not in use, some pH meters must be immersed to special solutions to prevent electrodes from degradation. Finally, they are fragile, since they have glass components, as well as they are power-consuming, meaning that batteries are needed, resulting in their limited portable use. In summary, conventional pH meters are quite effective tools for pH monitoring; however, they need special care during their use as well as when they are stored. Moreover, they exhibit limited portability and difficulty in remote operation.

In order to overcome such disadvantages, microwave metasurface-based pH sensors arise as very promising alternatives. In principle, a metasurface (MS) is a carefully engineered 2-dimensional structure, which can interact with microwave signals, giving rise to resonance behavior at certain frequencies [14, 15]. Such resonance behavior can be tuned by tailoring MS's dielectric surroundings, resulting in resonance frequency shifts and/or resonance intensity alterations, enabling its sensing capability [16–18]. Therefore, when interacting with a solution, the effective permittivity of the MS is influenced due to the complex dielectric permittivity of the solution, resulting in resonance behavior changes (either resonance frequency shift or resonance amplitude modulation). Apparently, the complex dielectric permittivity of the solution is related to its pH level, and therefore, any alteration of the resonance behavior is straightly correlated to pH, enabling MS's capability in pH detection [3, 19]. Such MS–based pH sensors exhibit distinctive advantages, such as practical sensing performance, miniaturization and versatility. They are easy-to-use, fast and responsive; they do not require neither regular calibration or special storage conditions; they are passive, needing no batteries and power supplies, and they can be remotely operated, giving real-time pH data.

Considering the above, there are quite a few reports in which MS–based structures are dedicated for pH detection [19–28]. All of them exhibit remarkable performance as electromagnetic sensors, with very high quality factor values, allowing the detection of pH changes either through resonance frequency shift [19, 21, 28], or resonance intensity [22, 27, 29]. In addition, some of them show considerable response in a wide pH region [20, 22, 24]. Apart from their significant pH sensing capabilities, such MS–based architectures include metasurfaces' advantages, offering high sensitivity, label-free sensing, miniaturization, fast response, passive operation, tunable properties, etc. All of the above-mentioned MS-based pH sensors have been grown using traditional Printed Circuit Board (PCB) technology. PCB method is conventionally employed for the development of high-quality metasurfaces. It consists of various development steps, namely chemical etching, milling, annealing, etc. In some of those steps, chemicals are used, with direct environmental consequences. Moreover, the corresponding infrastructure is expensive and complicated, while the personnel using such instrumentation must be trained. As a consequence, the development of metasurfaces, through the PCB process, becomes complicated.

In this context, other alternative approaches are proposed. Among them, additive/subtractive manufacturing [30–32] technology enables the capability to produce complex structures, with very precise dimensions. Moreover, it allows the easy, quick, and massive production of MSs, using ordinary, eco-friendly materials. In such way, the overall cost is reduced, industry-scale production can be achieved, while safe environmental conditions can be kept. Employing 3D printing technology, high-performance microwave sensors, based on metasurfaces, have been developed for various applications, including microfluidic [33] and biosensors [34, 35]. Moreover, 3D-printed potentiometric sensors have been constructed for pH detection [36–39]. Even more, 4D-printed complex star-like structures have been proposed for pH sensing [40]. Nevertheless, to the best of our knowledge, there is not any report on a microwave MS–based pH sensor, fabricated using additive/subtractive manufacturing technology.

Considering the above, we hereby propose an MS–based pH sensor, which has been developed employing the Computer Numerical Control (CNC) method. In contrast to conventional PCB fabrication routes [19–29], the proposed fabrication approach enables rapid prototyping, reduced fabrication complexity, lower production cost, and elimination of chemical etching steps, while maintaining sensing functionality comparable to previously reported SRR/metasurface architectures. Therefore, an alternative and environmentally friendly fabrication strategy for microwave pH sensing devices is proposed, based on an SRR-sensing topology, which has been previously evaluated regarding its real-life sensing performance [27, 33, 41, 42]. Thus, the present work does not introduce a new SRR/metasurface pH-sensing mechanism; instead, its novelty lies in the implementation of an established sensing concept using CNC-based subtractive manufacturing.

The developed sensor performs in the microwave regime (1–5 GHz), and it is connected to a portable vector network analyzer through a coaxial cable. The small dimensions of both the sensor and the analyzer make the system transferable, while the internal memory of the analyzer allows for data storage without the use of a laptop, if desired. With the use of a laptop, the whole system becomes remotely operated, allowing the data recording and transfer in long distances. Regarding its detection performance, the proposed sensor was tested against buffer solutions (stable solutions with accurately tuned pH levels, used for calibration of traditional electrode pH meters) as well as other aqueous solutions with pH ranging from 2 to 12. The sensor exhibited distinct behavior in varying pH levels, enabling its capability as pH sensor. The experimental results are corroborated by corresponding theoretical simulations. The overall performance of the sensors was determined through Quality Factor, Sensitivity, and Figure of Merit. All three quantities are comparable with others reported for microfluidic and pH sensors, based on microwave resonators. Overall, the proposed sensing device shows distinct

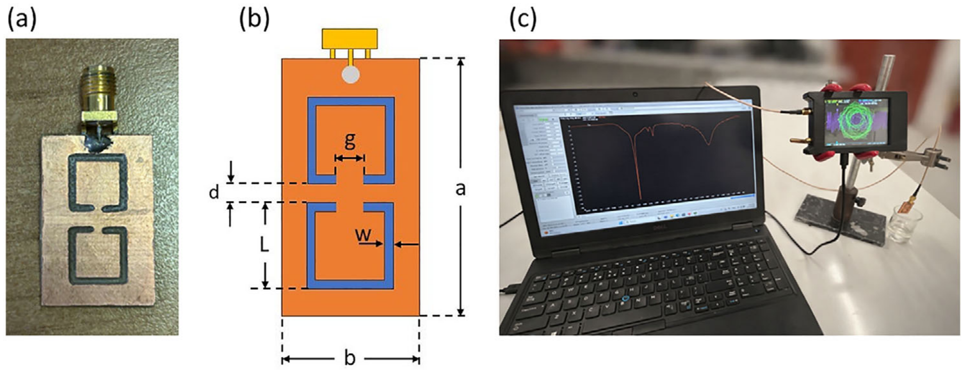

FIGURE 1 | (a) Constructed pH device used in the current study. (b) pH device drawing. Corresponding dimensions are shown. (c) Experimental set-up used in the current study. The VNA is placed on the stand. The pH device is hanged above a beaker, containing the solution under test. The software used for monitoring the electromagnetic response of the pH device, is shown in the laptop. The whole set-up is completely portable.

pH– dependent electromagnetic behavior, enabling its potential use of pH monitoring applications. Portability adds another positive option in the overall result, and shows the way for in-field pH sensing applications.

2 | Experimental Details

2.1 | Metasurface Fabrication

In the current study, an MS was developed, employing CNC mechanical engraving, which is a subtractive fabrication process that uses rotating cutting tools to remove material from a workpiece. The CNC milling system typically consists of a worktable for positioning the workpiece, a cutting tool, and an overhead spindle for securing and rotating the cutting tool. In general, the worktable can be moved in both x and y axes while the spindle with the cutting tool can be moved along the z axis. The spindle with the attached cutting tool rotates at several hundreds of rpms. Thus, by the combined movement of both the worktable and the spindle, the cutting tool digs the workpiece at specific areas, so as the desired object is formed. Usually, CNC is employed in manufacturing metal, plastic, and wooden parts, with various cutting tools, such as lathes, mills, drills, etc.

In the current study, a complementary double Split Ring Resonator (CSRR) topology is chosen for the meta-atom (Figure 1b). Such a topology has been recently proposed for the detection of pollutants in water [42], as well as in quality control in food products [41, 43]. The complementary structure of the MS also favors the employment of the CNC engraving, toward a high-quality, PCB-like MS. Moreover, complementary MSs behave similarly to the MS, albeit they are the "negative counterpart" of them. The analogy in the response between of them is described by the Babinet principle [44].

Typical double side copper coated FR-4 board was used as the engraving surface. A TTC450 Engraving machine (TELOS TRADING LIMITED, UK), equipped with an 80 W CNC module, was used for the engraving process. Appropriately designed MS drawings were developed using the open-source CAD software EASEL (Inventables Inc., Chicago, IL, USA). Apart from the CAD files, this software is capable of producing the corresponding g-code files needed for guiding the engraver's movements, while it can also be used for the automatic operation of the engraver. In the rotating spindle, a carpenter blade was attached, 1 mm in diameter. The spindle moves in all three directions, and as soon as the rotating carpenter blade touches the FR-4 surface, it removes certain areas of the copper coating, according to the desired CAD drawing. For the purposes of our studies, the engraving depth was kept at 0.2 mm. Employing the above-described process, an engraved MS is constructed, as shown in Figure 1a. The SRRs are appropriately oriented so that their gaps are opposite to each other. In such a configuration, each SRR couples with its neighbor, enhancing the electric field into the gap, and thus the EM behavior of the MS is improved. SRR dimensions are shown in Figure 1b, i.e., L = (10.1 ± 0.1) mm, w = (1.40 ± 0.06) mm, g = (1.5 ± 0.2) mm, d = (3.48 ± 0.06) mm; the whole MS is a = (30.0 ± 0.1) mm long and b = (20.0 ± 0.1) mm wide.

2.2 | pH Sensor Construction

Figure 1a shows a picture of the proposed pH device. A SMA connector is attached to the printed MS. The center contact is attached to the MS surface while the outer shell is connected to the back-plate of the MS. Such topology allows to excite the resonances of the meta-atom via a coaxial cable instead of using free-space beams or a rectangular waveguide setup.

2.3 | Electromagnetic Characterization of pH Sensor

The constructed sensor was electromagnetically characterized in ambient atmosphere. In particular, the device was connected to a portable vector network analyzer – VNA (LightVNA 64, Shenzhen Henlifeng Electronic Commerce Co., Ltd, China), via an SMA–to–SMA cable (Figure 1c). The whole set-up was connected to a PC, and the free-released NanoVNA software (OneOfEleven, Sports management, Germany) was used to operate it. All operations and data acquisition functions were performed through the software. Using this experimental set-up, the complex-valued S_{11} parameter was recorded as a function of frequency, in the range 1–6 GHz.

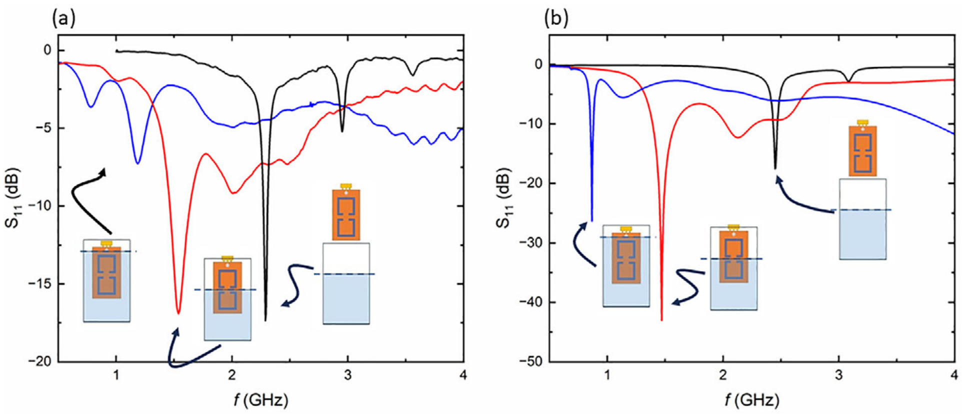

FIGURE 2 | (a) EM spectra of the pH device at various positions with respect to the solution surface. (b) Results from corresponding numerical simulations.

TABLE 1 | Buffer solutions as well as mixed solutions, used in the current study. Code names, measured pH values, suppliers, and Acetic acid / NaOH solution mixing ratios are given.

Solution		**pH (T = 25°C)**	**Supplier**
Buffer	PHA4	4.01	Omega Engineering LTD
	PHA7	7.00	Omega Engineering LTD
	PHA10	10.01	Omega Engineering LTD
			Acetic acid / NaOH ratio
Home-made	PH25	2.5	0.3 mL / 0.1mL
	PH51	5.1	0.1 mL / 13.7 mL
	PH62	6.2	0.01 mL / 19.3 mL
	PH77	7.7	Only water
	PH92	9.2	0 / 20 mL
	PH122	12.2	0 / 3.2 mL
	PH132	13.2	0 / 32 mL

2.4 | pH Sensing Experiments

Before testing against any acidic/basic solution, the device was tested with respect to water. Table water as used as test sample (Zaros natural mineral water, ZAROS S.A., Greece; pH = 7.7). The device was gradually immersed into the water, and corresponding EM spectra were recorded, with respect to the position of the device in relation to the water surface. Corresponding results are presented in Figure 2. As it will be discussed later, the optimum position is found to be when half of the device is immersed into the water.

After verifying the sensing reaction of the device in the presence of the water, its response to solutions with different pH levels is investigated. In this context, standard buffer solutions were used; these commercially available solutions exhibit accurately determined pH levels, and they are used for calibration of conventional potentiometric pH meters. Following a similar experimental procedure as previously described, the EM behavior of the device was recorded with respect to different buffer solutions, shown in Table 1.

Finally, the pH device was tested against home-made solutions. More specifically, the device was tested against aqueous solutions consisting of glacial acetic acid (A6283, Sigma–Aldrich Chemie GmbH, Germany, pH 2.5) and NaOH (S5881, Sigma–Aldrich Chemie GmbH, Germany). The latter material is in pellets; thus, a precursor aqueous solution was prepared, 1% w/v in concentration. This precursor solution was used to prepare other solutions with lower pH values, in combination with the acetic acid. All home-made solutions are of total volume of 50 mL, and the acetic acid / NaOH mixing ratios are presented in Table 1. The pH level of all solutions was measured using a traditional pH meter. Finally, in all aqueous solutions, table water was used as solvent.

2.5 | Dielectric Permittivity Measurements

The dielectric permittivity of all studied solutions was measured using the standard coaxial probe method. An open-ended coaxial probe (N1501A dielectric probe kit, Keysight Technologies, CA, USA) was connected to the P9372A VNA. The probe was immersed directly in each solution, and the dielectric permittivity (real and imaginary parts) was automatically calculated through the VNA software (N1500A Materials Measurement Software Suite, Keysight, California, USA), in the frequency regime 1–9 GHz. Corresponding spectra for both the real and imaginary parts of the dielectric permittivity of all solutions are shown in Figure S1.

2.6 | Theoretical Simulations

In parallel to the experimental results, numerical simulations were also performed. The full-wave simulations with continuous-wave (CW) excitation were performed using the frequency-domain solver of the commercial software CST Studio Suite. The pH−sensing antenna was designed on a FR−4 substrate (microwave permittivity 4.3 and loss tangent of 0.025) with standard copper (electric conductivity 58 MS/m) as metallization layers with 35 um thickness. The two split-rings were engraved on one side (dimensions shown on Figure 1b), and a lumped 50 Ohm port was used as the antenna feed. To compute the resonance behavior of the antenna, we place it in a cuboid domain enclosed by perfectly matched layers (PML), modeled via the 'open' boundary condition in CST; then, we excite the feed port and compute the reflection, which indicates if the antenna input impedance is matched. The operating band, where the antenna is most sensitive to its environment, is for the frequencies where we have a minimization of the backscattering into the feeding port, with $|S_{11}| < -10$ dB typically indicating good matching and antenna resonance.

Note that the environment of the antenna greatly affects its resonance frequency and bandwidth and that water at the microwave spectrum presents a high ($\varepsilon_r \approx 80$) and lossy ($\tan\delta \approx 0.1$) relative dielectric permittivity, meaning that the wavelength is nine times smaller than the vacuum wavelength.

3 | Results and Discussion

The black solid line in Figure 2a corresponds to the as-recorded EM response of the studied device in ambient atmosphere. A sharp dip is observed at 2.29 GHz, while other two broader minima are observed at 2.94 and 3.56 GHz, respectively. By immersing the device into the water, the spectrum is dramatically changed; i.e. a minimum at ~1.44 GHz with a satellite minimum at 2.01 GHz are observed (red line, Figure 2a). Both of them are broader than those in the black curve. By fully immersing the device into the water, both these dips further shift to lower frequencies (0.78 and 1.19 GHz), while they show lower intensity and even broader profiles (blue line, Figure 2a). No other dips are observed. The optimum position of the device into the water can be considered as the position in which it exhibits maximum sensing capability. In accordance, the sensing capability is closely related to the electromagnetic performance of the device, which can be expressed through the Quality Factor Q:

$$Q = \frac{f_{res}}{f_{3dB}} \tag{1}$$

where f_{3dB} is the 3 dB bandwidth and f_{res} is the frequency where the dip is observed [45, 46]. Corresponding values are listed in Table 2.

From the above calculated Q values it becomes clear that, as soon as the device is immersed into the water, its EM performance is severely reduced, reflecting the possibility that this proposed device may not be efficient for sensing applications in aqueous solutions, let alone detection of pH levels. Indeed, moderate Q values have been obtained for other MS-based sensors of similar topology [41–43]. However, in all cases the proposed MSs succeeded in the detection of tiny dielectric changes, so that they became potentially usable sensors for water and food quality control. In this context, their investigation regarding the detection of the pH level in aqueous acidic/alkaline solutions becomes prudent.

Corresponding numerical simulation results are shown in Figure 2b. In the case of the device in the ambient atmosphere, the produced simulated spectrum shows a sharp peak at ~2.45 GHz, with another satellite peak at ~3.08 GHz, very close to the peaks observed in Figure 2a. In the half-immersed position, the produced simulation spectrum exhibits a steep peak at ~ 1.47 GHz accompanied with another broad shoulder at ~2.13 GHz, closely following the experimental results. In the fully-immersed position, numerical simulations also show a peak below 1 GHz and another broad hump above 1 GHz however, their shape and intensity cannot be compared to the as-recorded spectrum of Figure 2a. In terms of EM performance (i.e., Table 2), Q takes its highest values in the half-immersed position, which is attributed to the very sharp and narrow dip, extracted from numerical simulations. Thus, numerical simulations succeeded to qualitatively describe the EM behavior of the sensing device.

Here it should be noted that a quantitative difference exists between simulated and experimental Q values, implying that there are several crucial factors influencing the experimental procedure, resulting the reduced Q, with respect to the numerical simulation-derived ones. For instance, fabrication tolerances introduced during the CNC fabrication process are a crucial parameter. As shown in Figure 1a, SRRs are appropriately printed with well-defined geometry; however, their corners are rounded, and the edges of the engraved areas are not perfectly straight and sharp, which could result in the reduction of the EM response. In addition, parasitic losses associated with the SMA connector and the coaxial cable can also contribute to the suppression of the EM signal of the device. Moreover, uncertainties in the dielectric properties of the liquid samples can also affect the EM performance of the proposed device, and consequently lead in reduced Q values. Nevertheless, both numerical simulations and experimental results reveal the half-immersed position as the most appropriate to be applied for sensing applications, for the investigated device.

In order to clarify the capability of the device to respond in solutions of varying pH levels, we tested it against buffer solutions PHA4, PHA7 and PHA10, respectively (Table 1). The corresponding EM response of the device is shown in Figure 3. In particular, Figure 3a, shows the EM response of the device, when half-immersed in those solutions. It is evidently shown that there are distinct EM spectra obtained for each buffer solution,

TABLE 2 | Resonance frequencies, f_{3dB}, and Q quantities, for all peaks observed in Figures 2a,b.

Position	f_{res} (GHz)	f_{3dB} (GHz)	Q	f_{res} (GHz)	f_{3dB} (GHz)	Q
		Experiment			Simulation	
Out of water	2.29	0.017	134	2.45	0.016	153
Half immersed	1.44	0.082	17.6	1.47	0.003	489
Fully immersed	0.78	0.174	6.81	0.867	0.003	289

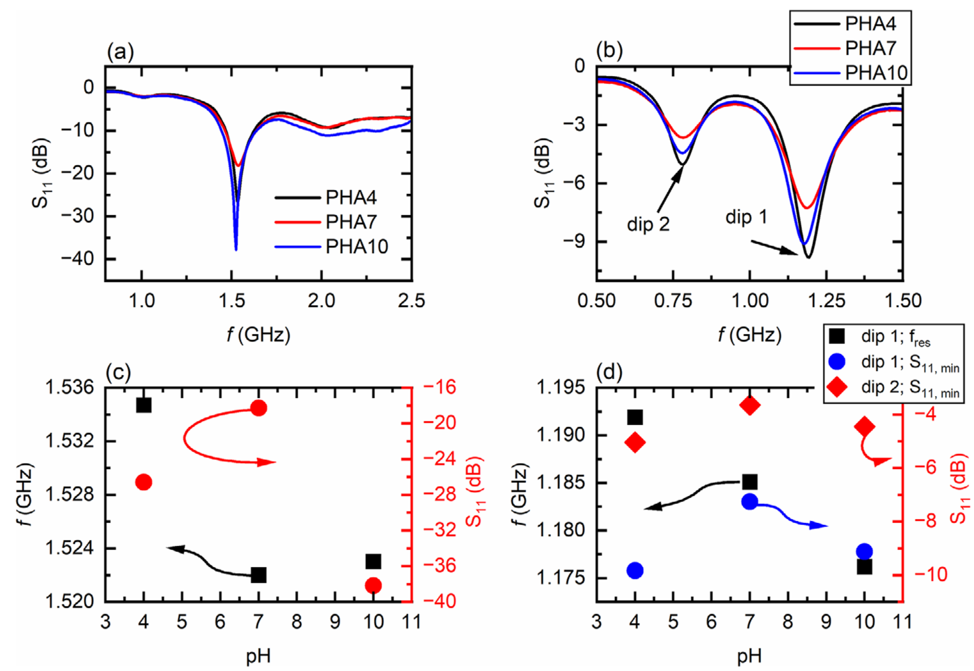

FIGURE 3 | Electromagnetic response of the device in the presence of buffer solutions of varying pH levels, when (a) it is half immersed and (b) when it is fully immersed. (c) Resonance frequency f (black symbols) and S_{11} intensity (red symbols) with respect to pH, as extracted from panel (a), when the sensor is half-immersed. (d) Resonance frequency f for dip 1 (black symbols), S_{11} intensity for dip 1 (blue symbols) and dip 2 (red symbols) with respect to pH, as extracted from panel (b), when the sensor is fully immersed.

i.e., for PHA4 (black line), PHA7 (red line), and PHA10 (blue line). In all cases a sharp dip is observed at 1.53 GHz. The reflection level is strongly affected by the pH level (black symbols, Figure 3c), since it is interrelated with the imaginary part of the dielectric permittivity (Figure S1b) and the fulfillment of the critical coupling condition. Deviations in the real part of the permittivity (Figure S1a) lead to a frequency shift, but they are rather weak in relative terms. In case the device is fully immersed into the solutions, two broad but distinct dips are observed (Figure 3b); one at 1.19 GHz, and another at 0.78 GHz. The reflection levels of both dips similarly vary with changing pH level (red and blue symbols, Figure 3d). The trend followed is qualitatively similar to that shown in Figure 3c, when the device is half-immersed into the solution, indicating a stable response in pH variations, regardless of the device position. From the above observations, it can be evidently assumed that the proposed device distinctly responds to buffer solutions with varying pH levels.

In general, frequency shifts are closely related to corresponding variations in the real part of the permittivity and changes in the minimum reflection level to changes in the imaginary part. Thus, it is crucial to investigate the variation of dielectric permittivity with respect to the pH level, in the frequency regime where the device resonates. The imaginary part of dielectric permittivity ε'' (Figure 4b, as it has been extracted from Figure S1b) gets its highest value for PHA7 solution, while it reaches low values for PHA4 and PHA10 solutions. Thus, the low ε'' values of the latter solutions, as well as the high ε'' of the PHA7, seem to be related to their EM behavior, namely, S_{11} becomes weaker for PHA7, while it is enhanced for PHA4 and PHA10 solutions (Figure 3b,d). In contrast, the real part of the dielectric permittivity ε' for all three buffer solutions (Figure 4a) shows a monotonic behavior, which cannot be correlated to the EM response of the device.

Considering the above discussion, it comes out that the proposed sensing device can distinguish among solutions with a wide range of varying pH levels, through S_{11} intensity variations, rather than through resonance frequency shifts. As shown in Figure 4b, the pH−induced modification of the aqueous medium predominantly affects the imaginary part of the dielec-

TABLE 3 | Resonance frequencies, FWHM values and corresponding Q values for all buffer solutions, in two different positions of the device, with respect to the solution surface.

Device position	pH	f_{res} (GHz)	f_{3dB} (GHz)	Q
Half -immersed	4	1.53	0.023	66.4
	7	1.52	0.070	21.7
	10	1.52	0.008	185
Fully immersed (dip @ ~1.19 GHz)	4	1.19	0.086	13.8
	7	1.18	0.175	6.77
	10	1.17	0.107	11.0

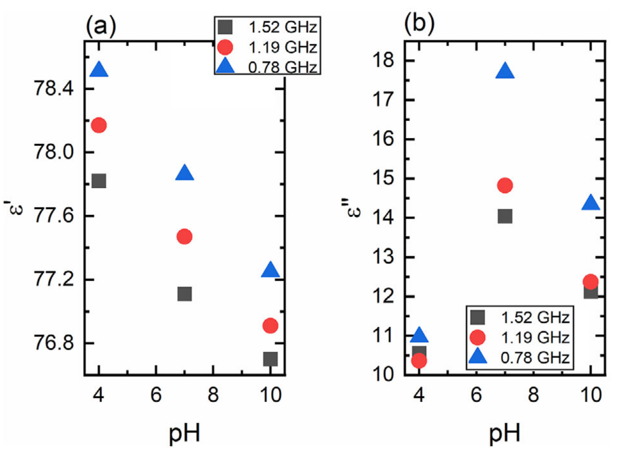

FIGURE 4 | (a) Real part of the dielectric permittivity as a function of pH level, for f = 1.54 GHz (black symbols) and f = 1.19 GHz (red symbols), respectively. (b) Corresponding imaginary part of the dielectric permittivity as a function of pH level, for both frequencies.

tric permittivity, whereas the real part weakly varies (Figure 4a) with pH. Thus, pH mainly modulates the resonant dissipation, giving rise to pronounced changes in the minimum S_{11} intensity, while the resonance frequency slightly shifts. Therefore, in the proposed sensing configuration, the S_{11} amplitude provides a larger dynamic range and a more robust calibration parameter than the resonance frequency itself. Such a behavior has also been previously seen for other resonating pH sensors [22, 23, 26, 27].

The efficiency of the device as a pH sensor can be determined through the Quality Factor. In Table 3, Q values for all buffer solutions, in all immersion positions, are listed. It is clearly seen that for the PHA7 solution, which shows the lowest ε'', Q takes the lowest values, while for PHA4 and PHA10 (high ε''), Q increases significantly, giving credence to the capability of the sensor to detect pH changes. Moreover, Q values are higher when the device is half immersed in the solutions, due to the sharp and deep spectra obtained. When the sensing device is fully immersed in solutions, dips become broader and shallower, resulting in low Q values. Thus, the half-immersed position is confirmed as the most relevant configuration for reliable pH measurements when using the proposed sensing device.

After the evaluation of the sensor with respect to buffer solutions, it is prudent to investigate its response to real alkaline / acidic solutions such as those listed in Table 1. Figure 5a shows the electromagnetic signal obtained with the device half-immersed into solutions, with increasing pH levels. A well-defined dip is observed at around 1.55 GHz, which becomes stronger as pH increases toward pH = 7, and then it weakens as the solution becomes more alkaline (pH > 7). Such behavior is apparent in Figure 5b, in which the S_{11} dip intensity is shown with respect to the pH level. A decreasing trend is observed in the acidic regime, while an increasing trend is shown in the alkaline region. A similar trend has been reported for frequency shift in other resonator-based pH sensors [20, 21, 47, 48]. As it has been previously discussed, solutions' dissipation losses result in the tunable S_{11} intensity.

Sensitivity of the proposed sensing device can be determined through the slope in the S_{11} vs pH diagram [22]. In this context, data are well-fitted to linear regression, with corresponding slopes and R^2 coefficients listed in the next table (Table 4), for both acidic and alkaline regions.

For basic solutions, positive slope for $S_{11,\min}$ is observed, in contrast to the acidic solutions. In addition, S_{11} slopes are equal (absolute values), within the calculated error. R^2 values are comparable of even higher compared to those reported in the literature [19, 22, 28, 49], for other resonator-based pH sensors. Comparing to other devices, the sensitivity of which is determined through the S_{11} vs. pH curve, the hereby proposed set-up shows comparable performance [8, 19, 22, 23, 50]. Therefore, the proposed MS-based device exhibits a consistent capability to distinguish and quantify pH levels for acidic/basic solutions, suggesting its potential use as pH sensor.

Corresponding numerical simulation results are also presented in Figure 5c, which qualitatively follow the experimental evidence. In particular, a minimum is observed at ~1.44 GHz, which becomes stronger as pH increases toward pH = 7, while it weakens as pH diverges from neutral value. Moreover, in Figure 5d, calculated S_{11} intensity is shown with respect to the pH level. A decreasing trend is observed for in the acidic regime, while an increasing trend is shown in the alkaline region. Therefore, numerical simulations qualitatively corroborate the experimental results.

We also examined thephase of S_{11} as a function of pH for home-made solutions (Figure S2a). The phase exhibits a pronounced dispersive transition at resonance frequency for all solutions. This transition becomes smoother for strongly acidic/alkaline

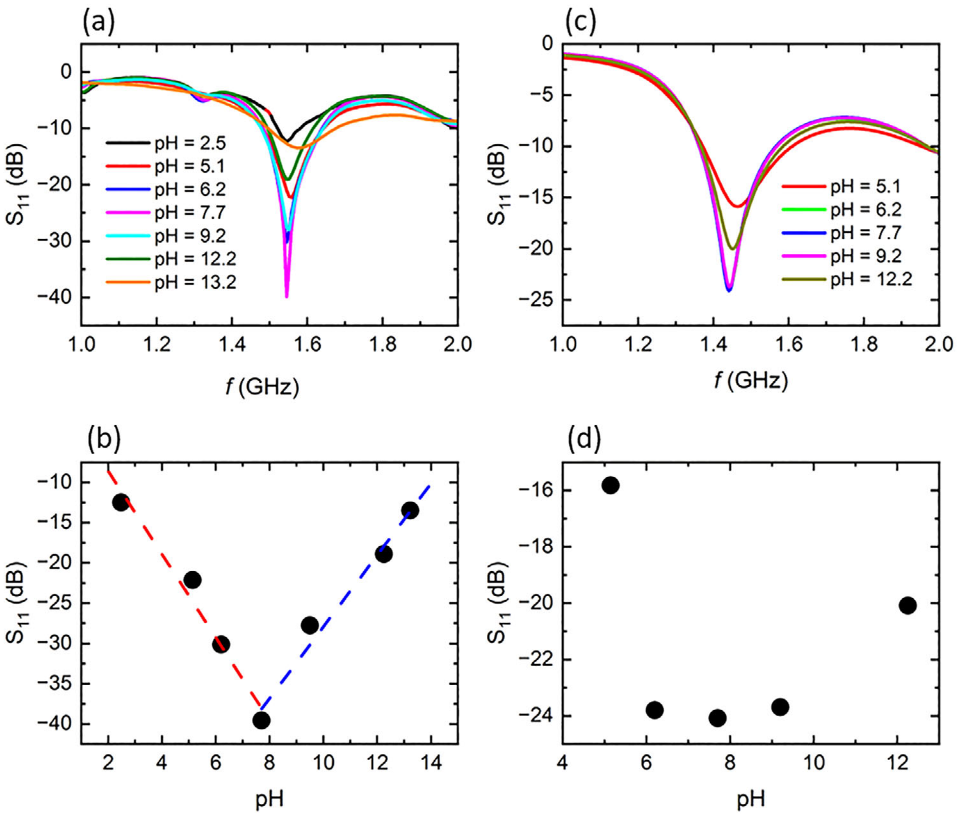

FIGURE 5 | S_{11} vs f spectra for solutions with varying pH in half-immersed position; (a) experimental results and (c) corresponding numerical simulations. (b) S_{11} intensity vs pH, as extracted from panel (a). (d) S_{11} intensity vs pH for, as extracted from panel (c).

TABLE 4 | Slope and R^2 values, from linear fittings presented in Figure 4b.

	$S_{11,\,min}$ slope (dB / pH) Experiment	R^2
Acidic solutions	$-(5.2 \pm 0.6)$	0.97
Basic solutions	4.5 ± 0.5	0.98

samples, while for samples near neutrality (pH ~ 7) the transition becomes steeper. However, for solutions with closely similar pH levels, the corresponding phase curves nearly overlap, making it difficult to resolve small pH differences. This behavior is also reproduced by the numerical simulations (Figure S2b), which qualitatively corroborate the experimental observations. Moreover, phase measurements are highly sensitive to external factors such as cable motion, connector repeatability, and residual calibration imperfections of the portable VNA. These factors significantly increase the measurement uncertainty and reduce the overall reliability of a phase-based interrogation scheme. In view of those findings, and considering that one of the main advantages of the proposed sensor is its simple and portable operation with straightforward interpretation by non-expert end users, we deliberately adopt the amplitude of S_{11}, as the primary sensing parameter for the proposed device.

As an MS–based sensor, the proposed device exhibits a distinct EM response. Thus, it is prudent to determine the EM efficiency of the device through Quality Factor Q, described in Equation (1),

TABLE 5 | Resonance frequencies, f_{3dB}, Q, ε', S(%) and FoM quantities, for all home-made solutions.

pH	f_{res} (GHz)	f_{3dB} (GHz)	Q	ε'	S (%)	FoM
2.5	1.538	0.049	31.4	79.4	2.6	53
5.1	1.551	0.036	43.1	78.7	0.73	20
6.2	1.536	0.016	96.0	79.3	1.9	119
7.7	1.542	0.005	308	79.5	—	—
9.5	1.535	0.022	69.8	79.3	2.3	104
12.2	1.543	0.045	34.3	78.9	1.1	25
13.2	1.552	0.164	9.46	78.8	0.9	5.5

Sensitivity *S(%)*, and Figure of Merit *FoM*, using the following equations:

$$S\ (\%) = 100 \times \frac{\left|f_o - f_{pH}\right|}{f_o \cdot \left|\varepsilon'_o - \varepsilon'_{pH}\right|} \tag{4}$$

$$FoM = \frac{S}{f_{3dB}} \tag{5}$$

where $f_o = 1.542$ GHz, is the resonance frequency of pure water (pH = 7.7), f_{pH} is the resonance frequency for each solution, f_{3dB} is the 3 dB bandwidth [45], ε'_{pH} is the dielectric permittivity of each solution, and $\varepsilon'_o = 79.5$ is the dielectric permittivity of table water (Figure S1c). All calculated quantities for each solution are presented in Table 5 (half -immersed device). Here it is useful to

TABLE 6 | Comparison of the electromagnetic performance of the proposed pH sensor and other microwave resonator-based pH sensors, existing in the literature.

	Q	MUT	S%	FoM
[19]	37	Acidic / alkaline solutions	N/A	N/A
[28]	619	Coco peat samples	5.14	> 3000
[51]	67–92	Water-ethanol solutions	0.063	N/A
[49]	124	DI water	N/A	N/A
[52]	113	Oil samples	0.3–1.5	70
[53]	24–40	Water-ethanol solutions	0.27	N/A
[25]	75–175	HCl solutions	N/A	N/A
	155–185	NaOH solutions	N/A	N/A
	50–160	NaCl solutions	N/A	N/A
[54]	20–49	Citric acid solutions	< 1.5	N/A
	46–60	Glucose	<1.5	N/A
	14–16	NaCl Solutions	<.5	N/A
[55]	20	Biomolecules	N/A	N/A
[56]	51	Several liquids	0.23	3.3
[57]	37.4	Solid materials	3.27	27
[58]	10–20	NH_3, Fe solutions	1.40–1.43	N/A
This work (half – immersed) (depended on pH)	9–308	Acidic / alkaline solutions	0.9–2.6	5.5–119

distinguish between the sensitivity, determined through the slope in the S_{11} vs. pH curve, and the sensitivity, calculated through the relation (4). The latter corresponds to the performance of the electromagnetic device, regardless of its use, while the former refers to the evaluation of the SRR−based pH sensor efficiency.

It is seen that *Q* and *FoM* show relatively high values for pH near 7, which is attributed to the fact that, corresponding S_{11} spectra exhibit sharp and narrow dips at such pH levels. As pH deviates from 7, S_{11} curves become broad and shallow, resulting in low *Q* and *FoM* values. Comparing to other microwave pH sensors, as well as microfluid and liquid sensing SRR−based devices (Table 6), it is seen that *Q* values obtained here are well above the average, indicating the competitive performance of the proposed device in pH sensing. Even more, calculated sensitivity *S%* is also higher than many others reported so far, while *FoM* is also above the average. All in all, the proposed sensor demonstrates a stable electromagnetic behavior with measurable pH−dependent response characteristics.

4 | Summary and Conclusions

In the current study, a microwave device, based on a metasurface, is proposed for potential pH sensing applications. The device includes a mm−scale double split ring resonator engraved on a double-sided Cu−coated FR−4 substrate. employing conventional Computer Numerical Control (CNC technology. By properly attaching an SMA connector on the SRR, a compact microwave resonator was realized, which has been electromagnetically characterized both in ambient atmosphere and in contact to aqueous media. The device exhibits distinct resonance features at certain frequencies, in the range 1–5 GHz, and when half-immersed in water, it shows a sharp resonance dip around 1.44 GHz.

Upon exposure to buffer solutions of varying pH, the half-immersed configuration responds distinctly, showing comparatively high quality factor values. Similar behavior has been observed when the device is fully immersed in the solutions; however, its performance is drastically degraded. These findings indicate that the device can distinguish solutions of varying pH levels and that the half-immersed geometry is the most suitable configuration for reliable pH measurements.

Furthermore, the device was evaluated against home-made acidic and alkaline solutions, covering a broad pH range. It was found that the measured electromagnetic intensity varies linearly with pH changes, enabling quantitative pH estimation through simple amplitude analysis. The resulting pH sensitivity is comparable to other resonator pH sensors in the literature. In addition, the electromagnetic performance of the device was found to be all within the range of previously published metasurface and resonator architectures. Overall, the proposed sensor demonstrates reproducible pH-dependent electromagnetic behavior and practically useful sensitivity, without resorting to complex geometries or dedicated fabrication schemes.

In addition, it was shown that the employment of CNC−based subtractive fabrication can be realized as an efficient, environmentally friendlier, and cost-effective alternative to conventional PCB processing for metasurface pH sensors. The proposed fabrication route eliminates chemical etching steps, reduces process complexity, and enables rapid prototyping, while still yielding functional SRR-based devices with performance metrics comparable to related resonator pH sensors in the literature.

Moreover, the compact form of the whole sensing device, along with the use of a portable vector network analyzer, transforms the overall system into a portable and suitable platform for in-field pH monitoring applications. Taken together, these results indicate that CNC-fabricated metasurface devices constitute a practical and attractive platform for microwave pH sensing in aqueous environments.

Acknowledgements

The publication of the article in OA mode was financially supported by the Hellenic Academic Libraries Link (HEAL-Link).

Funding

The authors have nothing to report.

Conflicts of Interest

The authors declare no conflicts of interest

Data Availability Statement

All data supporting the findings of this study are available upon reasonable request.

References

1. A. Lokman, W. Z. Ismail, and N. A. Aziz, "A Review of Water Quality Forecasting and Classification Using Machine Learning Models and Statistical Analysis," *Water* 17 (2025): 2243.

2. A. E. Ben-Chioma, A. S. Jack, and G. S. Philipokere, "A Comparative Study on the Measurement of Ph of Water, Using Ph Metre and Water Testing Kit [Testube Method] in Port Harcourt," *International Journal of Applied Chemistry* 1 (2015): 1.

3. S. K. Dewangan, D. Toppo, and A. Kujur, "Investigating the Impact of pH Levels on Water Quality: an Experimental Approach," *International Journal for Research in Applied Science and Engineering Technology* 11 (2023): 756–759, https://doi.org/10.22214/ijraset.2023.55733.

4. L. M. Mosley, P. Rengasamy, and R. Fitzpatrick, "Soil pH: Techniques, Challenges and Insights from a Global Dataset," *European Journal of Soil Science* 75 (2024): e70021, https://doi.org/10.1111/ejss.70021.

5. S. K. Dewangan, S. Shrivastava, L. Kumari, P. Minj, J. Kumari, and R. Sahu, "The Effects of Soil Ph on Soil Health and Environmental Sustainability: a Review," *Journal of Emerging Technologies and Innovative Research* 10, no. 6 (2023): 611–616.

6. D. D. Zhou, *Biosensors and their Biomedical Applications*, ed. X. Zhang, H. Ju, and J.B.T.-E.S. Wang, (Academic Press, 2008), 261.

7. D. Goldoni, A. Ferrari, M. Piccini, S. Cattini, R. Molinari, and L. Rovati, "Blood-pH Optical Measurement: a Model to Compensate for the Effects of Temperature," *IEEE Transactions on Instrumentation and Measurement* 72 (2023): 1–8, https://doi.org/10.1109/TIM.2023.3250282.

8. R. E. Price, M. Longtin, S. Conley-Payton, et al., "Modeling Buffer Capacity and pH in Acid and Acidified Foods," *Journal of Food Science* 85 (2020): 918–925, https://doi.org/10.1111/1750-3841.15091.

9. T. Aydogdu, J. A. O'Mahony, and N. A. McCarthy, "pH, the Fundamentals for Milk and Dairy Processing: a Review," *dairying* 4 (2023): 395–409, https://doi.org/10.3390/dairy4030026.

10. K. D. Dolan and D. K. Mishra, "Parameter Estimation in Food Science," *Annual Review of Food Science and Technology* 4 (2013): 401–422, https://doi.org/10.1146/annurev-food-022811-101247.

11. S. Karastogianni, S. Girousi, and S. Sotiropoulos, "pH: Principles and Measurement," *Encyclopedia of Food and Healthed* 4 (2016): 333–338.

12. V. S. Kulkarni and C. Shaw, ed V.S. Kulkarni, and L.D. Shaw, "Miscellaneous Physical, Chemical, and Microbiological Test Methods, Essential Chemistry for Formulators of Semisolid and Liquid Dosages," Academic Press, 2016: 193–221, https://doi.org/10.1016/B978-0-12-801024-2.00011-X.

13. D. J. Rowe, S. Al-Malki, A. A. Abduljabar, A. Porch, D. A. Barrow, and C. J. Allender, "Improved Split-Ring Resonator for Microfluidic Sensing," *IEEE Transactions on Microwave Theory and Techniques* 62 (2014): 689–699, https://doi.org/10.1109/TMTT.2014.2299514.

14. A. Ali, A. Mitra, and B. Aïssa, "Metamaterials and Metasurfaces: a Review from the Perspectives of Materials, Mechanisms and Advanced Metadevices," *Nanomaterials* 12 (2022): 1027, https://doi.org/10.3390/nano12061027.

15. O. Tsilipakos, Z. Viskadourakis, A. C. Tasolamprou, et al., "Meta-Atoms with Toroidal Topology for Strongly Resonant Responses," *Micromachines* 14 (2023): 468, https://doi.org/10.3390/mi14020468.

16. S. Tabassum, S. K. Nayemuzzaman, M. Kala, A. Kumar Mishra, and S. K. Mishra, "Metasurfaces for Sensing Applications: Gas, Bio and Chemical," *Sensors* 22 (2022): 6896, https://doi.org/10.3390/s22186896.

17. Y. Wang, X. Zhang, Y. Wang, et al., "Recent Advances in Metasurfaces: From THz Biosensing to Microwave Wireless Communications," *Research* 8 (2026): 820, https://doi.org/10.34133/research.0820.

18. A. Xomalis, O. Tsilipakos, M. Manousidaki, et al., "Enhanced Refractive Index Sensing with Direction-Selective Three-Dimensional Infrared Metamaterials," *ACS Applied Optical Materials* 1 (2023): 10–16, https://doi.org/10.1021/acsaom.2c00001.

19. A. Musa, M. L. Hakim, T. Alam, et al., "Permeability Negative Split Square Resonator for Solid Materials Dielectric Constant and Aqueous Solution pH Sensing Applications," *Sensors and Actuators A: Physical* 369 (2024): 115107, https://doi.org/10.1016/j.sna.2024.115107.

20. Z. Abbasi and M. Daneshmand, "Contactless pH Measurement Based on High Resolution Enhanced Q Microwave Resonator," in *2018 IEEE/MTT-S International Microwave Symposium-IMS* (IEEE, 2018), 1156.

21. Z. Abbasi, H. Niazi, M. Abdolrazzaghi, W. Chen, and M. Daneshmand, "Monitoring pH Level Using High-Resolution Microwave Sensor for Mitigation of Stress Corrosion Cracking in Steel Pipelines," *IEEE Sensors Journal* 20 (2020): 7033–7043, https://doi.org/10.1109/JSEN.2020.2978086.

22. A. Bouchalkha and R. Karli, "Planar Microstrip Antenna Sensor for pH Measurements," in 2019 International Conference on Electrical and Computing Technologies and Applications (ICECTA) (IEEE, 2019): 1–5.

23. G. Gennarelli, S. Romeo, M. R. Scarfì, and F. Soldovieri, "A Microwave Resonant Sensor for Concentration Measurements of Liquid Solutions," *IEEE Sensors Journal* 13 (2013): 1857–1864, https://doi.org/10.1109/JSEN.2013.2244035.

24. D. Gustafson and D. Klyve, "Contactless Detection of pH Change in a Liquid Analyte," *Sensors* 25 (2025): 2832, https://doi.org/10.3390/s25092832.

25. H. Hamzah, J. Lees, and A. Porch, "Split Ring Resonator with Optimised Sensitivity for Microfluidic Sensing," *Sensors and Actuators A: Physical* 276 (2018): 1–10, https://doi.org/10.1016/j.sna.2018.03.023.

26. M. T. Islam, F. B. Ashraf, T. Alam, N. Misran, and K. B. Mat, "A Compact Ultrawideband Antenna Based on Hexagonal Split-Ring Resonator for pH Sensor Application," *Sensors* 18 (2018): 2959, https://doi.org/10.3390/s18092959.

27. K. Sakabe, T. Kan, and H. Onoe, "Entirely Biodegradable Wireless pH Sensor with Split-Ring Resonators for Soil pH Monitoring," *Advanced Materials Technologies* 9 (2024): 2400038, https://doi.org/10.1002/admt.202400038.

28. M. K. Uddin, T. Alam, M. L. Hakim, et al., "Polarization Insensitive Cross Resonator Based Highly Sensitive Metamaterial Absorber for pH Level Monitoring," *Optical Materials* 168 (2025): 117460, https://doi.org/10.1016/j.optmat.2025.117460.

29. M. R. Islam, M. T. Islam, M. S. M, et al., "Metamaterial Sensor Based on Rectangular Enclosed Adjacent Triple Circle Split Ring Resonator with Good Quality Factor for Microwave Sensing Application," *Scientific Reports* 12 (2022): 6792, https://doi.org/10.1038/s41598-022-10729-4.

30. K. Silver, J. Li, P. Dimitriou, C. Kallnik, A. Porch, and D. Barrow, "3D-printing Fabrication of Microwave-Microfluidic Device for Droplets Network Formation and Characterisation," *BioRxiv* 24 (2024): 5110.

31. J. Wang, R. Wang, Z. Shen, B. Liu, C. Sun, and Q. Xue, "Microwave Biosensors Utilizing Metamaterial Enhancement: Design and Application," *Nanotechnology and Precision Engineering* 8 (2024): 15001, https://doi.org/10.1063/10.0028757.

32. M. Esfandiari, J. Zhu, and Y. Yang, "Additively Manufactured Metasurfaces and Metamaterials: Designs, Fabrications, and Applications from Microwave to Photonics," *APL Photonics* 10 (2025): 41101, https://doi.org/10.1063/5.0241299.

33. A. Salim and S. Lim, "Complementary Split-Ring Resonator-Loaded Microfluidic Ethanol Chemical Sensor," *Sensors* 16 (2016): 1802, https://doi.org/10.3390/s16111802.

34. L. R. Silva, C. E. Lopes, A. A. Tanaka, L. M. Dantas, I. S. Silva, and J. S. Stefano, "Electrochemical Biosensors 3D Printed by Fused Deposition Modeling: Actualities, Trends, and Challenges," *Biosensors* 15 (2025): 57, https://doi.org/10.3390/bios15010057.

35. G. Remaggi, A. Zaccarelli, and L. Elviri, "3D Printing Technologies in Biosensors Production: Recent Developments," *Chemosensors* 10 (2022): 65, https://doi.org/10.3390/chemosensors10020065.

36. S. Lin, Y. Li, Z. Yang, et al., "Photopolymerization 3D-Printed Dual-Modal Flexible Sensor for Glucose and pH Monitoring," *Sensors* 25 (2025): 5358, https://doi.org/10.3390/s25175358.

37. A. Zalewska, N. Lenar, and B. Paczosa-Bator, "3D Printing in the Design of Potentiometric Sensors: a Review of Techniques, Materials, and Applications," *Sensors* 25 (2025): 4986, https://doi.org/10.3390/s25164986.

38. M. McCole, M. Bradley, M. McCaul, and D. McCrudden, "A Low-cost Portable System for on-site Detection of Soil pH and Potassium Levels Using 3D Printed Sensors," *Results in Engineering* 20 (2023): 101564, https://doi.org/10.1016/j.rineng.2023.101564.

39. M. Parrilla, A. Vanhooydonck, M. Johns, R. Watts, and K. De Wael, "3D-printed Microneedle-based Potentiometric Sensor for pH Monitoring in Skin Interstitial Fluid," *Sensors and Actuators B: Chemical* 378 (2023): 133159, https://doi.org/10.1016/j.snb.2022.133159.

40. C.-Y. Wu, J.-R. Chen, and C.-K. Su, "4D-printed pH Sensing Claw," *Analytica Chimica Acta* 1204 (2022): 339733, https://doi.org/10.1016/j.aca.2022.339733.

41. Z. Viskadourakis, A. Theodosi, K. Katsara, et al., "Engraved Split-Ring Resonators as Potential Microwave Sensors for Olive Oil Quality Control," *ACS Applied Electronic Materials* 6 (2024): 3846–3856, https://doi.org/10.1021/acsaelm.4c00430.

42. Z. Viskadourakis, G. Fanourakis, E. Tamiolakis, et al., "Fabrication of Mm-Scale Complementary Split Ring Resonators, for Potential Application as Water Pollution Sensors," *Materials* 16 (2023): 5290, https://doi.org/10.3390/ma16155290.

43. A. Drymiskianaki, K. Katsara, V. M. Papadakis, Z. Viskadourakis, and G. Kenanakis, "Engraved Microwave Metasurfaces for Potential Application in Honey Quality Control," *ACS Omega* 10 (2025): 46780–46793, https://doi.org/10.1021/acsomega.5c04380.

44. O. Tsilipakos, L. Maiolo, F. Maita, et al., "Experimental Demonstration of Ultrathin Broken-symmetry Metasurfaces with Controllably Sharp Resonant Response," *Applied Physics Letters* 119 (2021): 231601, https://doi.org/10.1063/5.0073803.

45. D. M. Pozar, *Microwave Engineering* (2011).

46. T. Christopoulos, O. Tsilipakos, G. Sinatkas, and E. E. Kriezis, "On the Calculation of the Quality Factor in Contemporary Photonic Resonant Structures," *Optics Express* 27 (2019): 14505, https://doi.org/10.1364/OE.27.014505.

47. X. Qiu, R. Tang, S. J. Chen, H. Zhang, W. Pang, and H. Yu, "pH Measurements with ZnO Based Surface Acoustic Wave Resonator," *Electrochemistry Communications* 13 (2011): 488–490, https://doi.org/10.1016/j.elecom.2011.02.028.

48. J.-C. Mau, G.-R. Lin, M.-Y. Fu, and W.-F. Liu, "A fiber Optic Sensor Based on Air-Gap Long Period Gratings for pH Sensing Application," *Microwave and Optical Technology Letters* 55 (2013): 855–857, https://doi.org/10.1002/mop.27466.

49. B. Camli, E. Altinagac, H. Kizil, H. Torun, G. Dundar, and A. D. Yalcinkaya, "Gold-on-glass Microwave Split-Ring Resonators with PDMS Microchannels for Differential Measurement in Microfluidic Sensing," *Biomicrofluidics* 14 (2020): 54102, https://doi.org/10.1063/5.0022767.

50. K. J. Dehning, M. Hitzemann, A. Gossmann, and S. Zimmermann, "Split-Ring Resonator Based Sensor for the Detection of Amino Acids in Liquids," *Sensors* 23 (2023): 645, https://doi.org/10.3390/s23020645.

51. F. Bagci, S. Can, M. S. Gulsu, A. E. Yilmaz, and B. Akaoglu, "A Microstrip-based Dielectric Sensor With Four Fluidic Channels for Complex Dielectric Constant Detection of Aqueous Alcohols," *Journal of Electromagnetic Waves and Applications* 38 (2024): 1635–1648, https://doi.org/10.1080/09205071.2024.2394433.

52. N. F. M. Razali, N. M. Sahar, A. Hoque, et al., "Compact Triple Decagon Split Ring Resonator Metamaterial for Liquid Sensing Applications," *Optical and Quantum Electronics* 56 (2024): 874, https://doi.org/10.1007/s11082-024-06811-y.

53. A. Kumar, M. S. Rajawat, S. K. Mahto, and R. Sinha, "Metamaterial-Inspired Complementary Split Ring Resonator Sensor and Second-Order Approximation for Dielectric Characterization of Fluid," *Journal of Electronic Materials* 50 (2021): 5925–5932, https://doi.org/10.1007/s11664-021-09099-w.

54. S. Harnsoongnoen, A. Wanthong, U. Charoen-In, and A. Siritaratiwat, "Planar Microwave Sensor for Detection and Discrimination of Aqueous Organic and Inorganic Solutions," *Sensors and Actuators B: Chemical* 271 (2018): 300–305, https://doi.org/10.1016/j.snb.2018.05.077.

55. H.-J. Lee, J.-H. Lee, H.-S. Moon, et al., "A Planar Split-ring Resonator-based Microwave Biosensor for Label-free Detection of Biomolecules," *Sensors and Actuators B: Chemical* 169 (2012): 26–31, https://doi.org/10.1016/j.snb.2012.01.044.

56. S. Agarwal and M. C. Garg, "Design of an Accurate, Planar, Resonant Microwave Sensor for Testing a Wide Range of Liquid Samples," *Electronics* 13 (2024): 4510.

57. K. Masrakin, S. Z. Ibrahim, H. A. Rahim, S. N. Azemi, P. J. Soh, and S. Tantiviwat, "Microstrip Sensor Based on Ring Resonator Coupled with Double Square Split Ring Resonator for Solid Material Permittivity Characterization," *Micromachines* 14 (2023): 790, https://doi.org/10.3390/mi14040790.

58. W. Ye, D.-W. Wang, J. Wang, G. Wang, and W.-S. Zhao, "An Improved Split-Ring Resonator-Based Sensor for Microfluidic Applications," *Sensors* 22 (2022): 8534, https://doi.org/10.3390/s22218534.

Supporting Information

Additional supporting information can be found online in the Supporting Information section.

Supporting File: adsr70179-sup-0001-SuppMat.docx.